Robotica (1997) volume 15, pp 313–318. Printed in the United Kingdom © 1997 Cambridge University Press

Variable structure control applied to underactuated robots

Kangsik Lee, Sheri Coates and Victoria Coverstone-Carroll

Department of Aeronautical and Astronautical Engineering, University of Illinois at Urbana-Champaign, 305A Talbot Laboratory, Urbana IL 61801 (USA). E-mail: Internet: vcc@uiuc edu

(Received in Final Form: June 8, 1996)

SUMMARY

Variable structure control is applied to an underactuated two and three-link robot. Control laws are developed to invert the robot from its stable, downward equilibrium position to an inverted position. This maneuver is accomplished by pumping energy into the system with the variable structure controller. A linear balancing controller is activated once the robot nears the inverted position. Numerical simulations are presented for both the two and three-link robot.

KEYWORDS: Underactuated robots; Variable structure control; Robots

INTRODUCTION

Underactuated mechanical systems are those that have fewer actuators than degrees of freedom. There are many examples of underactuated systems, including space robots,[1,2] flexible link robots, underactuated spacecraft[3–5] and systems that model both actuator and rigid body dynamics. The underactuated systems considered here are two and three-link planar robots where in both cases the first link has no direct control input. The plane of motion is parallel with the local gravity vector. The control problem consists of moving the robot from its stable downward position to the unstable inverted position and balancing it about this configuration.[6–9] This system is highly nonlinear and challenging to control. Recently, a combination of a nonlinear controller using Partial Feedback Linearization and a linear quadratic regulator was successfully applied to this problem and numerical results were presented for an underactuated two-link robot.[6,9] This paper presents an energy-based variable structure controller (VSC) that is utilized to drive the robot to a region near the unstable equilibrium where a linear quadratic regulator is employed to balance the robot. Numerical simulations for the two and the three-link robot are presented.

THE EQUATION OF MOTION OF THE UNDERACTUATED ROBOT

The equations of motion for the three-link revolute robot shown in Fig. [1] are given below. The first link is assumed passive (no direct control input) and the second and third links are active. The angular displacements of the three links are represented by the vector q and the angular velocities by the vector $\dot{q}$.

$$q = [q_1, q_2, q_3]^T \tag{1}$$

$$\dot{q} = [\dot{q}_1, \dot{q}_2, \dot{q}_3]^T \tag{2}$$

The equations of motion for the robot are written in Eqs. (3–5) and follow the nomenclature of Spong.[10] The variables τ_2 and τ_3 are the two control inputs. The Coriolis and centrifugal terms are contained in the h_i terms and the gravitational terms are represented by the ϕ_i terms. The equations of motion of the two-link system can be obtained through Eqs. (3)–(4) by setting the mass, inertia and length of the third link to zero.

$$m_{11}(q)\ddot{q}_1 + m_{12}(q)\ddot{q}_2 + m_{13}(q)\ddot{q}_3 + h_1(q, \dot{q}) + \phi_1(q) = 0 \tag{3}$$

$$m_{21}(q)\ddot{q}_1 + m_{22}(q)\ddot{q}_2 + m_{23}(q)\ddot{q}_3 + h_2(q, \dot{q}) + \phi_2(q) = \tau_2 \tag{4}$$

$$m_{31}(q)\ddot{q}_1 + m_{32}(q)\ddot{q}_2 + m_{33}(q)\ddot{q}_3 + h_3(q, \dot{q}) + \phi_3(q) = \tau_3 \tag{5}$$

where

$$\begin{aligned}
m_{11} &= m_1 l_{c1}^2 + m_2 l_1^2 + m_2 l_{c2}^2 + m_3 l_{c3}^2 + m_3 l_1^2 \\
&\quad + m_3 l_2^2 + 2m_2 l_1 l_{c2} \cos q_2 \\
&\quad + 2m_3 l_1 l_2 \cos q_2 + 2m_3 l_2 l_{c3} \cos q_3 \\
&\quad + 2m_3 l_1 l_{c3} \cos (q_2 + q_3) + I_1 + I_2 + I_3 \\
m_{12} &= m_2 l_{c2}^2 + m_3 l_{c3}^2 + m_3 l_2^2 + m_2 l_1 l_{c2} \cos q_2 + m_3 l_1 l_2 \cos q_2 \\
&\quad + 2m_3 l_2 l_{c3} \cos q_3 + m_3 l_1 l_{c3} \cos (q_2 + q_3) + I_2 + I_3 \\
m_{13} &= m_3 l_{c3}^2 + m_3 l_2 l_{c3} \cos q_3 + m_3 l_1 l_{c3} \cos (q_2 + q_3) + I_3 \\
m_{21} &= m_{12} \\
m_{22} &= m_2 l_{c2}^2 + m_3 l_{c3}^2 + m_3 l_2^2 + 2m_3 l_2 l_{c3} \cos q_3 + I_2 + I_3 \\
m_{23} &= m_3 l_{c3}^2 + m_3 l_2 l_{c3} \cos q_3 + I_3 \\
m_{31} &= m_{13} \\
m_{32} &= m_{23} \\
m_{33} &= m_3 l_{c3}^2 + I_3 \\
h_1 &= -m_2 l_1 l_{c2} \sin q_2 \dot{q}_2 (2\dot{q}_1 + \dot{q}_2) \\
&\quad - m_3 l_1 l_2 \sin q_2 \dot{q}_2 (2\dot{q}_1 + \dot{q}_2) \\
&\quad - m_3 l_2 l_{c3} \sin q_3 \dot{q}_3 (2\dot{q}_1 + 2\dot{q}_2 + \dot{q}_3) \\
&\quad - m_3 l_1 l_{c3} \sin (q_2 + q_3)(\dot{q}_2 + \dot{q}_3)(2\dot{q}_1 + \dot{q}_2 + \dot{q}_3) \\
\phi_1 &= (m_1 l_{c1} + m_2 l_1 + m_3 l_1) g \cos q_1 \\
&\quad + (m_2 l_{c2} + m_3 l_2) g \cos (q_1 + q_2)
\end{aligned}$$

https://doi.org/10.1017/S0263574797000350 Published online by Cambridge University Press

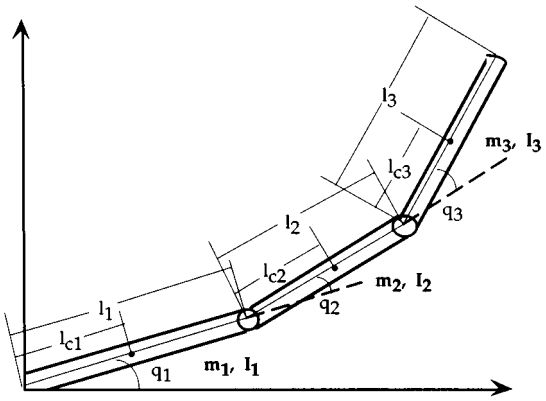


Fig. 1. The Three-Link Robot.

$$+ m_3 l_{c3} g \cos(q_1 + q_2 + q_3)$$

$$h_2 = m_2 l_1 l_{c2} \sin q_2 \dot{q}_1^2 + m_3 l_1 l_2 \sin q_2 \dot{q}_1^2 + m_3 l_1 l_{c3} \sin(q_2 + q_3)\dot{q}_1^2 - m_3 l_2 l_{c3} \sin q_3 \dot{q}_3 (2\dot{q}_1 + 2\dot{q}_2 + \dot{q}_3)$$

$$\phi_2 = (m_2 l_{c2} + m_3 l_2) g \cos(q_1 + q_2) + m_3 l_{c3} g \cos(q_1 + q_2 + q_3)$$

$$h_3 = m_3 l_1 l_{c3} \sin(q_2 + q_3)\dot{q}_1^2 + m_3 l_2 l_{c3} \sin q_3 (\dot{q}_1 + \dot{q}_2)^2$$

$$\phi_3 = m_3 l_{c3} g \cos(q_1 + q_2 + q_3)$$

VARIABLE STRUCTURE CONTROLLER

Variable structure control (VSC) design can be broken up into two distinct stages.[11] First, switching surfaces are chosen. A switching surface defines a relationship between state variables and is typically chosen to yield prescribed dynamics, such as desired orientation or angular velocity histories. The intersection of all the switching surfaces is referred to as the sliding manifold. A feedback control law is then designed to drive the state trajectories to the manifold and restrict them there. In this section, a sliding surface will be selected for a two-link underactuated robot and a controller will be explicitly derived. This discussion is followed by a general derivation of the nonlinear control law for the three-link underactuated robot.

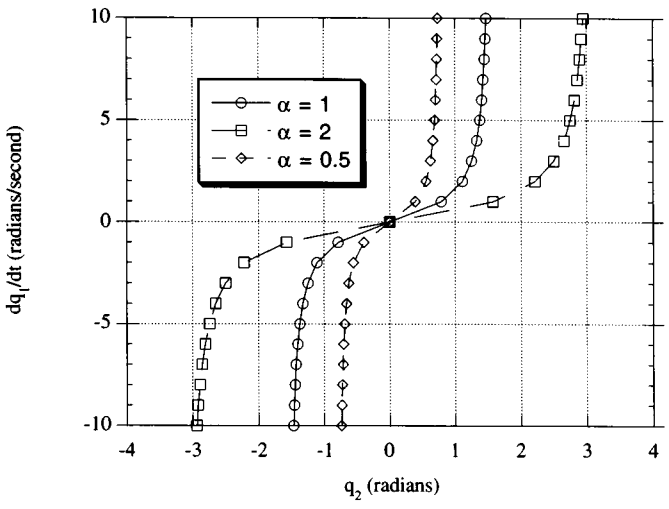


Fig. 2. The Sliding Surface for the Two-Link Robot.

1. Two-link VSC controller

The sliding surface used here relates the position of the second link to the velocity of the first link and is similar in concept to a person on a swing trying to build up energy. Just as the person swings their legs in the same direction as they are traveling, the motor rotates the second link to match the direction of the first link's velocity thereby pumping energy into the system. The sliding surface is shown in Eq. (6).

$$s = q_2 - \alpha \tan^{-1} \dot{q}_1 \tag{6}$$

The variable α is defined to be positive and affects the location of the asymptotes of the sliding surface. Figure 2 shows the sliding surface for three values of α. As α increases, the location of the asymptotes move away from the origin.

The controller is designed to drive the robot dynamics to the manifold ($s = 0$) and constrain them there. To design the controller, a positive definite Lyapunov function is defined in terms of the sliding manifold.

$$V(s) = \frac{s^2}{2} \tag{7}$$

The derivative of Eq. (7) is given in Eq. (8) where the time derivative of the sliding surface has been utilized.

$$\dot{V}(s) = s\left(\dot{q}_2 - \frac{\alpha \ddot{q}_1}{1 + \dot{q}_1}\right) \tag{8}$$

As previously mentioned, the equations of motion of the two-link system can be obtained through Eqs. (3)–(4) by setting the parameters involving the third link to zero. Equation (3) can be manipulated to yield an expression for the acceleration of link 1.

$$\ddot{q}_1 = -m_{11}^{-1}(m_{12}\ddot{q}_2 + h_1 + \phi_1) \tag{9}$$

Finally, Eq. (8) and Eq. (9) can be used to determine an expression for the derivative of the Lyapunov function.

$$\dot{V}(s) = s\left(\dot{q}_2 + \frac{\alpha m_{11}^{-1}(m_{12}\ddot{q}_2 + h_1 + \phi_1)}{1 + \dot{q}_1}\right) \tag{10}$$

The parameter m_{11} is positive definite and under the assumption that m_{12} is non-zero for all configurations, the control τ_1 is chosen so that the acceleration of link 2 is given in Eq. (11).

$$\ddot{q}_2 = -m_{12}^{-1}(h_1 + \phi_1) - \frac{m_{11} m_{12}^{-1}(1 + \dot{q}_1^2)}{\alpha}(\dot{q}_2 + ksgn(s)) \tag{11}$$

Combining Eqs. (10) and (11) yield a negative definite derivative for the Lyapunov function for $k > 0$.

$$\dot{V}(s) = -sksgn(s) < 0 \tag{12}$$

The *sgn* in Eqs. (11) and (12) is the signum function and returns the sign of s. Equation (12) is negative when the states are not on the sliding manifold and zero only when $s = 0$ (i.e. the system is on the sliding manifold). Therefore all system trajectories will move toward the attracting sliding surface. The nonlinear gain k affects the

https://doi.org/10.1017/S0263574797000350 Published online by Cambridge University Press

speed at which the system moves toward the manifold. The nonlinear VSC controller, τ_2, is given in Eq. (13).

$$\tau_2 = \bar{m}_{22}\ddot{q}_2 + \bar{h}_2 + \bar{\phi}_2 \tag{13}$$

When computing the torque, the acceleration of link 2 is given in Eq. (11) and the barred quantities are supplied below.

$$\bar{m}_{22} = m_{22} - m_{21}m_{11}^{-1}m_{12} \tag{14}$$
$$\bar{h}_2 = h_2 - m_{21}m_{11}^{-1}h_1 \tag{15}$$
$$\bar{\phi}_2 = \phi_2 - m_{21}m_{11}^{-1}\phi_1 \tag{16}$$

2. Three-link VSC controller

The three link robot requires a switching surface for each actuator. The two switching surfaces are defined generally as $f_1(q_1, \dot{q}_1)$ and $f_2(q_2, \dot{q}_2)$ where these surfaces are continuously differentiable functions of q and $\dot{q}$. The first surface relates the dynamics of the first two links and the second surface relates links two and three.

$$s_1 = q_2 - f_1(q_1, \dot{q}_1) \tag{17}$$
$$s_2 = q_3 - f_2(q_2, \dot{q}_2) \tag{18}$$

To design the control law, a Lyapunov function similar to the two-link example $V(s) = \frac{1}{2}s^Ts$ is used. Again, the controller is designed such that the derivatives of $V(s)$ are negative semi-definite along the system trajectories described in (3)–(5). The derivatives of $V(s)$ requires the derivative of the sliding surfaces:

$$s = \begin{bmatrix}\dot{s}_1\\ \dot{s}_2\end{bmatrix} = \boldsymbol{a}(\boldsymbol{q}, \dot{\boldsymbol{q}}) + \tilde{\boldsymbol{M}}(\boldsymbol{q}, \dot{\boldsymbol{q}})\begin{bmatrix}\ddot{q}_2\\ \ddot{q}_3\end{bmatrix} \tag{19}$$

where the vector $\mathbf{a}(\mathbf{q}, \dot{\mathbf{q}})$ and matrix $\tilde{\mathbf{M}}(\mathbf{q}, \dot{\mathbf{q}})$ are given below. In deriving Eq. (19), equation (3) was manipulated to yield an expression for $\ddot{q}_1$ and used in the expression for $\dot{s}_1$.

$$\boldsymbol{a}(\boldsymbol{q}, \dot{\boldsymbol{q}}) = \begin{bmatrix}\dot{q}_2 - \dfrac{\partial f_1}{\partial q_1}\dot{q}_1 + \dfrac{\partial f_1}{\partial \dot{q}_1}\left(\dfrac{h_1}{m_{11}} + \dfrac{\phi_1}{m_{11}}\right)\\ \dot{q}_3 - \dfrac{\partial f_2}{\partial q_2}\dot{q}_2\end{bmatrix} \tag{20}$$

$$\tilde{\boldsymbol{M}}(\boldsymbol{q}, \dot{\boldsymbol{q}}) = \begin{bmatrix}\dfrac{\partial f_1}{\partial \dot{q}_1}\dfrac{m_{12}}{m_{11}} & \dfrac{\partial f_1}{\partial \dot{q}_1}\dfrac{m_{13}}{m_{11}}\\ \dfrac{-\partial f_2}{\partial \dot{q}_2} & 0\end{bmatrix} \tag{21}$$

The sliding surfaces are selected such that $\tilde{\boldsymbol{M}}^{-1}(\boldsymbol{q}, \dot{\boldsymbol{q}})$ exists. Now, torques are generated such that:

$$\ddot{\boldsymbol{q}}_a = \begin{bmatrix}\ddot{q}_2\\ \ddot{q}_3\end{bmatrix} = \tilde{\boldsymbol{M}}^{-1}(\boldsymbol{q}, \dot{\boldsymbol{q}})(-Ksgn(s) - \boldsymbol{a}(\boldsymbol{q}, \dot{\boldsymbol{q}})) \tag{22}$$

where K is a diagonal positive definite matrix and *sgn* is the signum function defined as:

$$sgn(s_i) = \begin{pmatrix}+1 \text{ if } s_i \geq 0\\ -1 \text{ if } s_i < 0\end{pmatrix} \tag{23}$$

Finally, Eq. (22) is combined with (19) to yield the sliding surface derivative below.

$$\dot{s} = -Ksgn(s) \leq 0 \tag{24}$$

The Lyapunov function derivative then becomes negative semi-definite.

$$\dot{V} = s^T\dot{s} = -s^TKsgn(s) \leq 0 \tag{25}$$

Since $\dot{V}$ is zero only on the sliding surfaces ($s_i = 0$), all system trajectories move toward and terminate on the sliding manifold. Therefore, q_2 will converge to $f_1(q_1, \dot{q}_1)$ and q_3 to $f_2(q_2, \dot{q}_2)$. The torques required to drive the system to the manifold are computed by substituting Eq. (22) into Eq. (26).

$$\bar{\boldsymbol{M}}_{22}\ddot{\boldsymbol{q}}_a + \bar{h}_a + \bar{\phi}_a = \tau \tag{26}$$

where

$$\bar{\boldsymbol{M}}_{22} = \boldsymbol{M}_{22} - \frac{\boldsymbol{M}_{21}\boldsymbol{M}_{12}}{\boldsymbol{M}_{11}} = \begin{bmatrix}m_{22} - \dfrac{m_{12}^2}{m_{11}} & m_{23} - \dfrac{m_{12}m_{13}}{m_{11}}\\ m_{23} - \dfrac{m_{12}m_{13}}{m_{11}} & m_{33} - \dfrac{m_{13}^2}{m_{11}}\end{bmatrix} \tag{27}$$

$$\bar{h}_a = h_a - \frac{\boldsymbol{M}_{21}h_1}{\boldsymbol{M}_{11}} = \begin{bmatrix}h_2 - \dfrac{m_{12}h_2}{m_{11}}\\ h_3 - \dfrac{m_{13}h_1}{m_{11}}\end{bmatrix} \tag{28}$$

$$\bar{\phi}_a = \phi_a - \frac{\boldsymbol{M}_{21}\phi_1}{\boldsymbol{M}_{11}} = \begin{bmatrix}\phi_2 - \dfrac{m_{12}\phi_1}{m_{11}}\\ \phi_3 - \dfrac{m_{13}\phi_1}{m_{11}}\end{bmatrix} \tag{29}$$

In the simulations that follow, the sliding surfaces are selected as in Eqs. (30) and (31) where $a = 0.4$ seconds.

$$s_1 = q_2 - a\dot{q}_1 \tag{30}$$
$$s_2 = q_3 - a\dot{q}_2 \tag{31}$$

LINEAR QUADRATIC REGULATOR

Once the robot is close to the vertical configuration, control of the robot is switched to a linear control law to capture and balance the robot. A Linear Quadratic Regulator (LQR) is used to accomplish this task.[12] To this end, the robot dynamics are linearized about the vertical equilibrium resulting in a controllable linear system.

$$\dot{\boldsymbol{x}} = \boldsymbol{A}\boldsymbol{x} + \boldsymbol{B}\boldsymbol{u} \tag{32}$$

For the three-link robot, the state vector $\boldsymbol{x} = [q_1 - \pi/2 \quad q_2 \quad q_3 \quad \dot{q}_1 \quad \dot{q}_2 \quad \dot{q}_3]^T$, the control input $\boldsymbol{u} = [\tau_2 \quad \tau_3]^T$, and the matrices $\boldsymbol{A}$ and $\boldsymbol{B}$ are 6×6 and 6×2 matrices resulting from the linearization about the vertical configuration. A similar system can be obtained for the two-link robot where $\boldsymbol{x} = [q_1 - \pi/2 \quad q_2 \quad \dot{q}_1 \quad \dot{q}_2]^T$ and $u = \tau_2$.

A LQR controller is easily designed using the computer software Matlab. The state feedback controller $\boldsymbol{u} = -\boldsymbol{K}\boldsymbol{x}$ results where $\boldsymbol{K}$ is 2×6 gain matrix for the three-link robot and a 1×4 gain matrix for the two-link robot.

https://doi.org/10.1017/S0263574797000350 Published online by Cambridge University Press

Table I. Two-Link Simulation Parameters.

Parameter	m_1(kg)	m_2(kg)	l_1(m)	l_2(m)	l_{c1}(m)	l_{c2}(m)	I_1(kg-m^2)	I_2(kg-m^2)	g(m/s^2)
Experimental	0.873	1.1	0.254	0.295	0.16	0.241	0.0352	0.298	9.81

SIMULATIONS

With the equations of motion and control algorithms for the VSC and LQR derived, the software SIMNON (Simulation Language for Non-linear Systems) is used to integrate the set of nonlinear equations. The two-link swing-up simulations are discussed first.

1. Two-link simulation

Before the simulations can proceed, values for the robot parameters must be defined. The parameters used are shown in Table I and are based on an underactuated two-link experimental robot that has recently been built. The next step was to find the best combination of nonlinear and linear gains that would swing the robot up to the desired position and stabilize it. A variety of α's and k's were tried and it was determined that $\alpha = 1$ and $k = 0.4$ swung the robot up to the capture region the quickest. Once the robot was in the capture region, the nonlinear controller was replaced with the LQR. The A and B matrices needed for the LQR are given equations (33) and (34).

$$A = \begin{bmatrix} 0 & 1 & 0 & 0 \\ 31.262 & 0 & -4.186 & 0 \\ 0 & 0 & 0 & 1 \\ -29.906 & 0 & 12.150 & 0 \end{bmatrix} \tag{33}$$

$$B = \begin{bmatrix} 0 \\ -10.230 \\ 0 \\ 14.896 \end{bmatrix} \tag{34}$$

The weighting matrices were chosen to be $R = 10$ and Q to be the four-by-four identity matrix. Matlab then yields the gain matrix shown below.

$$K = [-35.9786 \quad -10.3600 \quad -13.9865 \quad -5.8552] \tag{35}$$

Figure 3 shows the link displacements for this two-link simulation. The LQR was turned on at 18.4 seconds. The initial conditions for the robot arm are $q_1(0) = -89.9$ and $q_2(0) = 0$ degrees and both initial angular velocities equal to zero. It can be seen that with each swing, the angular displacement of the links increase until the LQR is initiated. The nonlinear controller is increasing the energy with each swing cycle. Figure 4 displays the torque profile for this simulation. Note that the torque demands are relatively small except for the peak torque of 17.6 Nm that occurs immediately after the linear controller is turned on. The reason for this is that when the LQR is initiated, the VSC has developed enough energy for the robot to not only reach the inverted position but to continue swinging around. Therefore, the LQR acts as a brake on the system. The magnitude of the maximum required torque is important since the motor associated with the experimental system has a peak deliverable torque of 25 Nm. Fortunately, this constraint is not violated during the simulation.

Simulations were also run for various initial displacements of both link 1 and link 2. In all cases, an initial displacement farther away for the stable equilibrium decreased the swing up time for the robot. This is easily explained due to the fact that any displacement adds energy to the system and therefore requires less time for the system to gain sufficient energy to swing up. One thing to note is that when $|q_2(0)| > 90$ degrees, a problem with the definition of the sliding surface in equation (6) develops. The principal value of the arctan function is

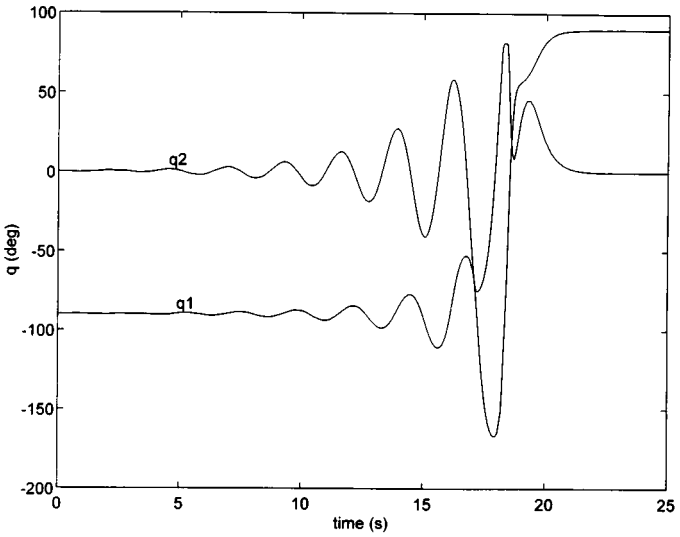


Fig. 3. Angular Displacements For Two-Link Swing Up.

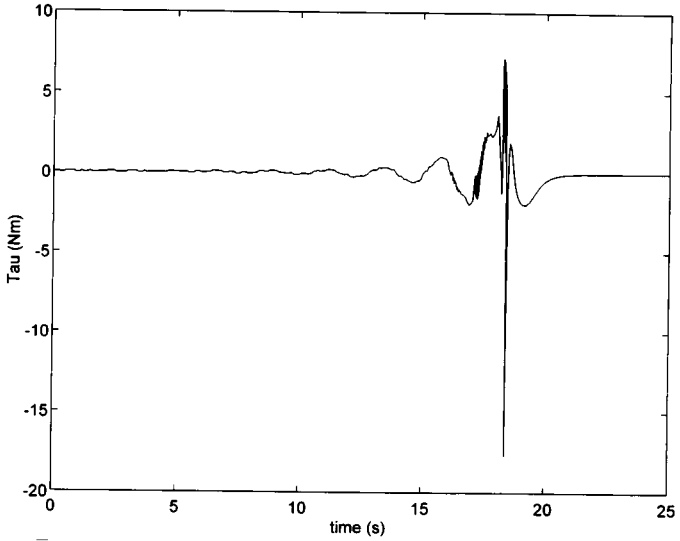


Fig. 4. Torque Profile For Two-Link Swing Up.

https://doi.org/10.1017/S0263574797000350 Published online by Cambridge University Press

Table II. Three-Link Simulation Parameters.

Parameter	m_1(kg)	m_2(kg)	m_3(kg)	l_1(m)	l_2(m)	l_3(m)
Theoretical	1	1	1	1.55	3.47	3.47

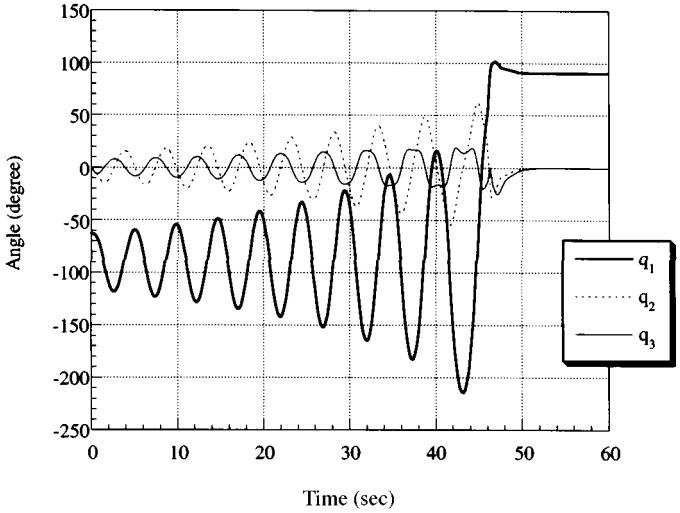


Fig. 5. Angular Displacements for the Three-Link Swing Up.

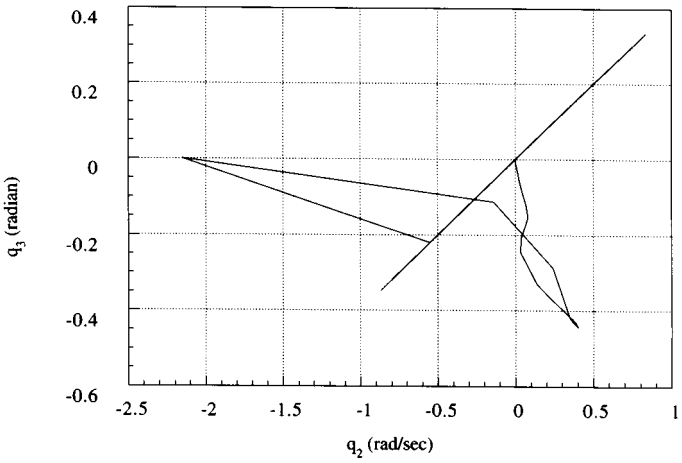


Fig. 7. The Sliding Surface, s_2.

always in the first and fourth quadrants but when $|q_2(0)| > 90$, the initial value of q_2 is in the second or third quadrants. There are two remedies to this situation. The first is to select a value for α sufficiently large enough to encompass the initial q_2. See Figure 2. If $\alpha = 2$, then all initial q_2 are included. The second solution is to let gravity naturally pull link 2 down and back into the principal value region of the arctan function. This solution is identical to just delaying the beginning of the swing up maneuver to a time when $|q_2(0)| < 90$ degrees. Several additional two-link simulations and the associated trends are described in more detail by Coates.[13]

2. Three-link simulation

Values for the robot physical parameters must be defined and are shown in Table II. These numbers do not correspond to an actual robot. The links are modeled as a uniform thin rod so that the moments of inertia are determined by $I_i = \frac{1}{12} m_i l_i^2$ and the length l_{ci} by $l_i/2$ $(i = 1, 2, 3)$. Also, to reduce the total time required to swing the robot up, the initial value of q_1 corresponds to about -63 degrees (-1.1 radians.) For this simulation, the switching surface s_1 is selected as $q_2 - 0.4\dot{q}_1$ and s_2 as $q_3 - 0.4\dot{q}_2$. Figure 5 shows the angular displacements of the links. As with the two-link simulation, the amplitudes of the link displacements increase with each swing until sufficient energy is built up and the LQR can be initiated. The LQR is switched on after 46 sec. Figures 6 and 7 show the switching surfaces for this simulation. Note that the switching surfaces are linear as defined until the LQR is turned on and the system reaches the origin when completely swung up. Figure 8 shows the torque profile.

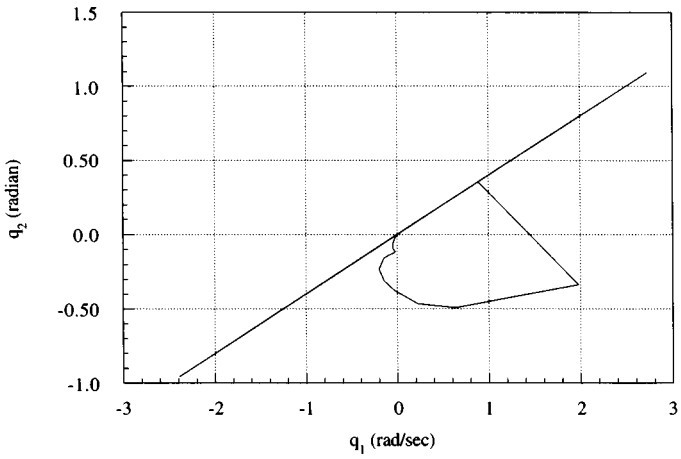


Fig. 6. The Sliding Surface, s_1.

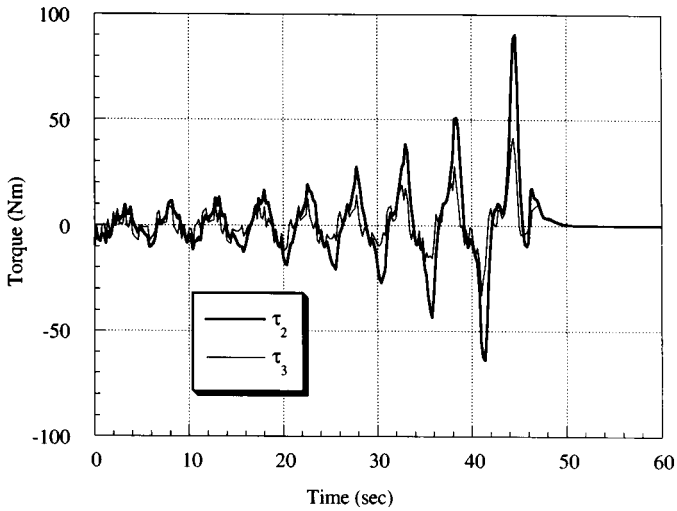


Fig. 8. Torque Profile For the Three-Link Swing Up.

https://doi.org/10.1017/S0263574797000350 Published online by Cambridge University Press

The torques gradually increase and peak before the LQR switching time. The high frequency component in the torques is due to the discontinuity (*sgn* term) in the VSC control algorithm. Also, the maximum torque is quite high due to the large robot parameters given in Table II.

CONCLUSIONS

Numerical simulations have shown that variable structure control (VSC) can be used to swing up a two and three-link underactuated robot. The VSC provides a mechanism to pump energy into the system until the robot is near the inverted configuration where a linear quadratic regulator is initiated. In the near future, the variable structure controller will be applied to an experimental underactuated two and three-link robot. It is anticipated that the VSC approach will provide a control algorithm that will be robust to unmodeled dynamics and parameter uncertainties.

References

1. A. Jain and G. Rodrigues, ''An Analysis of the Kinematics and Dynamics of Underactuated Manipulators'' *IEEE Transactions on Robotics and Automation* **9,** No. 4, 411–422 (August, 1993).
2. R. Mukhergee and D. Chen, ''Control of Free-Glying Underactuated Space Manipulators to Equilibrium Manifolds'' *IEEE Transactions on Robotics and Automation* **9,** No. 5, 561–570 (October, 1993).
3. C. Byrnes and A. Isidori, ''On the Attitude Stabilization of Rigid Spacecraft'' *Automatica* **27,** No. 1, 87–95 (1991).
4. H. Krishnan, M. M. Reyhanoglu and H. McClamroch, ''Attitude Stabilization of a Rigid Spacecraft Using Two Control Torques: A Nonlinear Control Approach Based on the Spacecraft Attitude Dynamics'' *Automatica* **30,** No. 6, 1023–1027 (1994).
5. V. Coverstone-Carroll, ''Detumbling and Reorienting an Underactuated Rigid Spacecraft'' *Guidance, Control, and Dynamics* **19,** No. 3, 708–710 (May-June, 1996).
6. M.W. Spong, ''The Swing Up Control Problem For The Acrobot'' *IEEE Control Systems Magazine* **15,** No. 1, 49–55 (February, 1995).
7. R. Mukherjee and P. Jordan, ''Feedback Control of a Three-Link Planar Underactuated Manipulator Using a 'Surge' Velocity'' *Proceeding of the ASME Winter Annual Meeting, Aerospace Structures*: *Nonlinear Dynamics, and System Response* **AD-Vol. 33,** 85–94 (1993).
8. M. Bergman and Y. Xu, ''Robust Control of Underactuated Manipulators: Analysis and Implementation'' *Proceedings of the IEEE International Conference on Systems, Man, and Cybernetics,* Vol. 1 (1994), **Vol. 1,** pp. 925–930.
9. M.W. Spong, ''Partial Feedback Linearization of Underactuated Mechanical Systems'', *Proceedings of the IEEE International Conference on Intelligent Robots and Systems* (1994), **Vol. 1,** pp. 314–321.
10. M.W. Spong and M. Vidyasagar, *Robot Dynamics and Control* (John Wiley and Sons, New York, 1989).
11. J-J. Slotine and W. Li, *Applied Nonlinear Control* (Prentice Hall, N.J., 1991).
12. C-T. Chen, *Linear System Theory and Design* (Saunders College Publishing, 1984).
13. S. Coates, ''Control of an Underactuated Two-link Manipulator'' *M.S. Thesis,* University of Illinois at Urbana-Champaign, 1996).

https://doi.org/10.1017/S0263574797000350 Published online by Cambridge University Press